Research Paper

Near-Infrared Light Triggered ROS-activated Theranostic Platform based on Ce6-CPT-UCNPs for Simultaneous Fluorescence Imaging and Chemo-Photodynamic Combined Therapy

Caixia Yue[1,2], Chunlei Zhang[1], Gabriel Alfranca[1], Yao Yang[1], Xinquan Jiang[3], Yuming Yang[1✉], Fei Pan[1], Jesús M. de la Fuente[1] and Daxiang Cui[1,4✉]

1. Institute of Nano Biomedicine and Engineering, Key Laboratory for Thin Film and Microfabrication Technology of the Ministry of Education, Department of Instrument Science & Engineering, School of Electronic Information and Electrical Engineering, Shanghai Jiao Tong University, Shanghai 200240, P. R. China;
2. School of Biomedical Engineering, Shanghai Jiao Tong University, Shanghai 200240, P. R. China;
3. Department of Prosthodontics, Oral Bioengineering and Regenerative Medicine Lab, Ninth People's Hospital Affiliated to Shanghai Jiao Tong University, 639 Zhizaoju Road, Shanghai 200011, P. R. China.
4. National Center for Translational Medicine, Collaborative Innovational Center for System Biology, Shanghai Jiao Tong University, Shanghai 200240, P. R. China.

✉ Corresponding authors: E-mail: yumingyang@sjtu.edu.cn or dxcui@sjtu.edu.cn.

Abstract

Many drug controlled release methods have been integrated in multifunctional nanoparticles, such as pH-, redox-, temperature-, enzyme-, and light-responsive release. However, few report is associated with the ROS responsive drug controlled release. Herein, a thioketal linker-based ROS responsive drug (camptothecin conjugated with thioketal linker, abbreviated as TL-CPT) was prepared and the thioketal linker could be cleaved by ROS(reactive oxygen species). To achieve cancer simultaneous optical imaging, photodynamic therapy and chemotherapy, the photosensitizer Chlorin e6(Ce6), TL-CPT and carboxyl-mPEG were loaded on the upconversion nanoparticles (UCNPs), which were named as Ce6-CPT-UCNPs. Under 980 nm laser irradiation, Ce6-CPT-UCNPs emitted a narrow emission band at 645-675 nm which was overlapped with Ce6 absorption peak. Ce6 absorbed the light to produce ROS, which was used for photodynamic therapy and to cleave the thioketal linker in Ce6-CPT-UCNPs to release camptothecin for chemotherapy. Meanwhile, Ce6 absorbed the light, was used for near-infrared fluorescence imaging. The *in vivo* biodistribution studies showed that the prepared nanoparticles had high orthotopic lung cancer targeting efficiency. The *in vivo* therapeutic results demonstrated that NCI-H460 lung cancers could be completely eliminated by combining chemo- and photodynamic therapy under 980 nm laser irradiation. The prepared multifunctional Ce6-CPT-UCNPs have great potential in applications such as cancer targeted fluorescent imaging, simultaneous ROS activated chemo- and photodynamic therapy in near future.

Key words: ROS-sensitive nanoparticles, photodynamic therapy, Camptothecin, UCNPs, orthotopic lung cancer.

Introduction

Over the past several decade years, more and more research have been focused on multifunctional nanoparticles as platforms for simultaneous cancer diagnosis and drug delivery due to their distinguished advantages [1, 2]. By combining imaging probes with therapeutic drugs in the same platform, the tumor can be precisely delineated, and the optimal drug dose as well as therapeutic time can be determined by acquiring real-time drug distribution information *in vivo*[3, 4]. So far, the method based on

multifunctional nanoparticles combined with diagnosis and therapy has been termed as "nanotheranostic".

After cancer diagnosis is confirmed, chemotherapy is the commonest method for cancer therapy. To obtain the best curative effect and to avoid toxic side effects, many nanoparticles were developed to deliver drugs with cancer targeting abilities and controlled on-demand release properties. Many controlled release methods have been used in drug release, such as pH-, redox-, temperature-, enzyme-, and light-responsive release [5-10]. However, up to date, few reports are closely associated with ROS responsive drug control release. Recent reports reveal that thioketal groups can be readily cleaved by reactive oxygen species (ROS)[11, 12], which inspire us to explore ROS-responsive controlled drug release both in space and time.

Cancer cells exhibit greater ROS stress than normal cells, partly due to oncogenic stimulation, increase metabolic activity and mitochondrial malfunction. However, normal cells with lower basal stress and maintenance appear to have a higher capacity to fight against additional ROS-generating insults than cancer cells [13]. Therefore, the elevation of ROS around tumor environment can selectively kill cancer cells. Photodynamic therapy has been successfully utilized for the treatment of skin diseases in clinic and further extended to cancer therapy through generation of ROS to destroy cancer cells under the light irradiation of photosensitizers [14-16]. Not only ROS produced by photosensitizers can be used for photodynamic therapy, but also it can also cleave thioketal groups to release drugs. Thus, it is very necessary to develop a platform to combine ROS-responsive chemotherapy and photodynamic therapy with near-infrared or visible light imaging under laser irradiation. Singlet oxygen is one type of ROS, and Chlorin e6 (Ce6), as a second-generation photosensitizer with 650-750nm fluorescence emission, has been frequently used for photodynamic therapy [6], and has high singlet oxygen quantum yield.

In recent years, upconversion nanoparticles (UCNPs), typically lanthanide (Ln^{3+})-doped nanocrystals, have attracted significant interest in many areas including panel display and biomedical imaging [17]. Our groups have synthesized some kinds of UCNPs for tumor targeted imaging and therapy [18-20]. Less than 980 nm laser excitation, UCNPs emit visible or NIR light with narrow spectrum bandwidth, exhibiting unique optical characteristics such as minimized auto-fluorescence background, resistance to photobleaching, as well as increased light penetration depth in biological tissues [21]. In addition, UCNPs display good biocompatibility compared with quantum dots composed of toxic heavy metal ions such as Cd^{2+}[22]. It has been found that functionalized ultra-small UCNPs could be gradually excreted from reticuloendothelial systems (RES) without causing noticeable toxicity to the treated animals [23]. All those results have shown that UCNPs own great potential in applications such as molecular imaging and tumor therapy [24-26]. Up to date, the multifunctional UCNPs have been successfully used for photodynamic therapy and simultaneous optical imaging in cell and animal levels [21, 24, 27]. Most photosensitizers for photodynamic therapy are activated by visible light or 500-700 nm light, and have a limited penetration depth in live tissues [28]. When UCNPs are combined with photosensitizers, the NIR-to-visible upconversion capability of UCNPs can be used to excite photosensitizers through energy transfer, and then further activate loaded drugs in the deep tissue [21].

To achieve the goal of UCNPs used for simultaneous optical imaging, photodynamic therapy and ROS-responsive chemotherapy, NCI-H460 lung cancer cell line was selected as therapeutic target, a new multifunctional UCNPs system was fabricated. In this system, UCNPs were loaded with mPEG-COOH, photosensitizer Ce6, and ROS-cleavable thioketal-conjugated camptothecin. Under 980 nm laser irradiation, UCNPs can convert 980 nm light to 645 nm-675 nm light, which can active Ce6 on the nanoparticles via fluorescence resonance energy transfer(FRET), generating ROS, the ROS can be used for photodynamic therapy and cleave the thioketal linker in thioketal-conjugated camptothecin to release camptothecin for chemotherapy. Meanwhile, Ce6 has a fluorescence emission between 650-750 nm and can be used for fluorescence imaging (as shown in Fig.1). Overall, the prepared multifunctional UCNPs exhibit great potential in applications such as simultaneous photodynamic therapy, chemotherapy, and fluorescent imaging in lung cancer.

Materials and methods

Materials

Rare earth oxides Y_2O_3 (99.999%), Yb_2O_3 (99.999%), Er_2O_3 (99.999%), Tm_2O_3 (99.999%), 3-mercaptopropionic acid, triethylamine(TEA), 4-dimethylamiopryidine(DMAP), and camptothecin (CPT), were purchased from Aladdin Reagent Co. Ltd. (Shanghai, hina). Oleyl amine (OM) (>90%) was obtained from Alfa. Aesar Ltd. Trifluoroacetic acid (99%) was supplied by Sinopharm Chemical Reagent Co. Ltd. (Shanghai, China). 2,4,6-trichlorobenzoyl chloride and methoxyl-PEG-carboxyl (mPEG-COOH, MW≈2K) were obtained from J&K Chemical Reagent

Co. Ltd.(Shanghai, China). Chlorin e6 (Ce6) was purchased from Frontier Scientific (Utah, USA). Ln(CF3COO)₃ (Ln = Y, Yb, Tm and Er) were prepared with the literature method[29].

Synthesis of UCNPs

The UCNPs synthesis was carried out following a literature protocol [17]. First, 4 mmol of CF_3COONa and 2 mmol (total amounts) of $Ln(CF_3COO)_3$ (Ln: 78mol%Y+20mol%Yb+1.6 mol%Er+0.4 mol%Tm) were added to 20 mL oleylamine (OM) in a 100 mL three-neck round-bottom flask at room temperature. Next, the reaction solution was directly heated to 120°C to remove water and oxygen, with vigorous magnetic stirring in nitrogen for 1 hour. At this point, the reaction mixture was a transparent solution. And then the solution was heated to 320 °C under nitrogen at a rate of 10°C per minute and maintained at this temperature for 1 hour. After the reaction was completed, 10 mL of cyclohexane was poured into the solution at room-temperature. The resultant mixture was separated by centrifugation (11250g, 10 min at 20°C), washed with cyclohexane and chloroform three times and dried in vacuum at room temperature overnight.

Synthesis of ROS-cleavable TL and ROS-sensitive camptothecin pro-drug TL-CPT

In a typical reaction, a mixture of anhydrous 3-mercaptopropionic acid (5.2 g, 49.1 mmol) and anhydrous acetone (5.8 g, 98.2 mmol) were saturated with dry hydrogen chloride and stirred at room temperature for 4 h. After the reaction, the flask was stopped and chilled in an ice-salt mixture until crystallization was complete. The crystals were filtered, washed with hexane and cold water, the thioketal linker product was acquired after vacuum-freeze-dried (78%). ¹H NMR (400 MHz, DMSO-d_6, δ): 2.74 (t, 4H), 2.50 (t, 4H), 1.53 (s, 6H).

To synthesize ROS-sensitive camptothecin pro-drug TL-CPT (camptothecin conjugated with thioketal linker, abbreviated as TL-CPT), TL (252.1 mg, 1.0 mmol) was dissolved in anhydrous DMF (5mL). The solution of triethylamine (TEA,303.6mg,3.0mmol), 2,4,6-trichlorobenzoylchloride (241.9mg,1.0mmol), 4-dimethylamiopryidine (DMAP,24.4mg,0.2mmol) in anhydrous DMF (5 mL) was added to the above mentioned solution and the resulting solution was stirred at room temperature for 10 min. Next, the solution of camptothecin (174.1 mg, 0.5 mmol) in 10mL anhydrous DMF was added and the reaction was stirred for 24 h at room temperature. After that, the reaction was quenched with water and extracted with CH_2Cl_2 for 5 times. The combined organic layers were washed with brine for 5 times, dried

over Na_2SO_4 and concentrated to the crude product, which was purified by silica gel chromatography (CH_2Cl_2/CH_3OH:from 20:1 to15:1 and then 10:1 ratio in sequence) to give the desired product (70% yield).¹H NMR (400 MHz, DMSO-d_6, δ): 8.67(s,1H),8.08-8.11(q,2H),7.83(t,1H),7.68(t,1H),7.20(s, 1H),5.47(s,2H),5.28-5.34(q,2H),2.75-2.88(m,4H),2.66(t,2 H),2.38(t,2H),2.10-2.13(q,2H),1.54(s,3H),1.47(s,3H),0.9 0(t,3H).

Preparation of Ce6-CPT-UCNPs

TL-CPT (0.06mmol, 34.9mg), mPEG-COOH (0.15mmol, 300mg) and UCNPs (10mg) were added to 3mL DMF, and then the mixture was ultrasonicated for 10 min at 150W. After that, Ce6(0.015mmol, 9mg) was added to the mixture and ultrasonicated for 5 min, followed with stirring for 1 h at room temperature. Next, the mixture was centrifuged three time (11250g, 10 min every time), and the collected solid was repeatedly washed with water. Finally, the prepared nanoparticles (Ce6-CPT-UCNPs) were resuspended in deionized water.

Characterization of UCNPs and Ce6-CPT-UCNPs

The size and morphology of the UCNPs were characterized by TEM on a JEM-2100F system (JEOL, Japan) and SEM on a FESEM system (ZEISS, Germany). XPS experiments were carried out on an Axis Ultra DLD system (Shimadzu/ Kratos Analytical Ltd., Japan). FTIR spectra were performed using Nicolet 6700 spectroscope (Thermo Fisher Ltd., USA) with KBrpellets. The upcoversion luminescence emission spectra were recorded on a Hitachi FL-4600 spectrofluorometer, but the excitation source was an external 0-2W adjustable 980nm semiconductor laser with an optic fiber accessory, instead of the Xeon lamp in the spectrofluorometer. ¹H NMR spectra were measured on a Bruker AvanceⅢ 400 MHz spectrometer. Dynamic light scattering (DLS) measurements were performed using a NiComp380ZLS Zeta Potential/Particle sizer (PSS Nicomp, Santa Barbara, USA). Zeta-potential measurements were carried out on a Malvern Zetasizer Nano ZS90system. The UV/Vis absorption spectra were measured on the Varian cary 50 UV-VIS spectrophotometer.

Measurement of ROS-responsive TL-CPT degradation *in vitro* and CPT release from Ce6-CPT-UCNPs

The degradation of thioketal linkages in TL-CPT under ROS condition was investigated by incubating TL-CPT (10.82 µmol of thioketal groups) in a mixture of DMF (0.8mL) and water (0.2mL) with H_2O_2 (400 mM)and 3.2µM $CuCl_2$ at 37°C for 48 h. Then 7 mL

water was added to the solution and the product was precipitated. The product was centrifuged, washed with water for 2 times and dried in vacuum. The disappearance of the thioketal linkage peak (δ 1.47,1.54 ppm) was quantified by using ^{1}H NMR (400 MHz, DMSO-d_6).

In vitro release of CPT from the Ce6-CPT-UCNPs was studied in a release medium (phosphate buffered saline, PBS, pH 7.4) using dialysis bag (molecular weight cutoff of 3,500 Da). The Ce6-CPT-UCNPs was kept in dark as control.Ce6-CPT-UCNPs or Ce6-CPT-UCNPs/ Vitamin C were dissolved in the release media with a power of 600 mW/cm²980 nm laser irradiation for 30 min. Next, the three group nanoparticles were introduced into their respective dialysis bags. Sealed the dialysis bag, placed it in 20 mL of release medium in 50 mL centrifuge tube, and incubated at 37°C shaken with 200 rpm in dark. At desired time intervals, 1 mL of the external buffer was taken out and replenished with an equal volume of fresh medium. The concentration of CPT in the release medium was then measured by UV-Vis spectra absorption at 360 nm with DMSO added.

Cell viability assays of UCNPs and the therapeutic evaluation of Ce6-CPT-UCNPs *in vitro*

NCI-H460 human lung cancer cells were acquired from the Cell Bank of Chinese Academy of Sciences. NCI-H460 cells (1×10⁴ cells per well) were seeded in 96-well plates and incubated overnight at 37 °C with 5% CO_2 in RPMI-1640 medium, supplemented with 10% FBS, 100 U/mL penicillin and 0.1mg/mL streptomycin. After being rinsed with PBS, the cells were incubated with 100μl of different concentration of UCNPs (10μg/ml, 20μg/ml, 50μg/ml, 100μg/ml, 200μg/ml and 500μg/ml) for 24h, then MTT (tetrazolium salt) assay was applied to evaluate the effect of UCNPs on NCI-H460 cells by measuring the uptake and reduction of tetrazolium salt to an insoluble formazan dye by cellular microsomal enzymes.

To evaluate photodynamic therapeutic efficacy of the Ce6-CPT-UCNPs in vitro, NCI-H460 cells (5×10³ cells per well) were seeded onto 96-well plates and incubated for 24 h. Then, culture media in the wells were respectively replaced with 100μL medium of containing free CPT, Ce6-UCNPs or Ce6-CPT-UCNPs, followed by 4 h incubation at 37 °C in the dark, and then Ce6-UCNPs or Ce6-CPT-UCNPs groups were irradiated with 980 nm laser, 0.6 W/cm² for 20 min with a 1 min interval after each minute of irradiation. After another 18 h of incubation in the dark, cell viability was measured by MTT assays.

To evaluate chemotherapeutic and photody-

namic therapeutic efficacy of Ce6-CPT-UCNPs, NCI-H460 cells were seeded onto a 24-well plate (7 x 10⁴cells per well) and incubated for 24 h. The medium was replaced with fresh medium containing Ce6-CPT-UCNPs(15μg/mL of free Ce6 equivalents). After 4h incubation in the dark, the NCI-H460 cells were half-covered and irradiated with 980 nm laser, 0.6 W/cm² for 20 min with a 1 min interval after each minute of irradiation. After another 2h of incubation in the dark, the cells were washed with PBS and stained with calcein-AM and PI. Calcein-AM-stained cells were alive, while PI-stained cells were dead. A confocal laser scanning microscope (CLSM) was utilized to detect cellular uptake and distribution of Ce6-CPT-UCNPs in NCI-H460 cells. The cells were plated on 14 mm glass cover slips and allowed to adhere for 24h. Then, the medium was changed to fresh medium containing Ce6-CPT-UCNPs (10 μg/mL of free Ce6 equivalent). After 4 h incubation, the cells were washed twice with PBS and fixed with 4% paraformaldehyde solution for 20 min. Then the nuclei were stained with Hoechst 33258 (10μg/mL). Finally, the fixed cells were observed by CLSM (Leica TCS SP8, Germany). The excitation wavelength and emission spectrum of each of the fluorescent indicators were as follows: Hoechst 33258 was excited with 406 nm, and the fluorescence emission was collected from 425 to 460 nm, Ce6 was excited with 633 nm laser, and the emitted light was collected from 650 to 800 nm.

Measurement of intracellular ROS in lung cancer cells treated with Ce6-CPT-UCNPs

After NCI-H460 cells were incubated withCe6-CPT-UCNPs (5μg/mL of free Ce6 equivalents) for 24 h in 12-well plate, the cells were further incubated with 20 μM DCFH-DA for 20 min and irradiated using a 980 nm laser, 0.6 W/cm² for 8 min with a 1 min interval after each minute of irradiation. The intracellular ROS generation was measured by staining all the cells with DCFH-DA. Subsequently, the fluorescence intensity of DCF inside the cells was detected by flow cytometry, which was proportional to the amount of ROS produced.

Preparation of orthotopic and subcutaneous lung tumor mouse model

Female BALB/cathymic nude mice (5 weeks old and weighted 17-20 g) were purchased from Shanghai Slac Laboratory Animal Co. Ltd. (Shanghai, China) and all animal experiments were carried out in compliance with the Institutional Animal Care and Use Committee of Shanghai Jiao Tong University (no. SYXK2007-0025). To establish the orthotopic NCI-H460 lung tumor model, the mice were anesthetized and the chest wall was sterilized with 70% al-

cohol. A 5-7 mm skin incision was made in the chest at the dorsal mid axillary line just below the inferior border of the scapula (about 1.5 cm above the lower rib line).While monitoring the motion of the left lung, 1×10^6cells in a mixture of 40μLPBS were injected slowly into the lung parenchyma. The incision was closed with sutures. The mice were kept warm to recover and tumor growth was examined at 2 weeks after inoculation. For the establishment of the NCI-H460 subcutaneous xenografted tumor model, NCI-H460 cells (1×10^6) were administered by subcutaneous injection into the right flank of the mice.

Ce6-CPT-UCNPs for *in vivo* fluorescence imaging and biodistribution on orthotopic lung cancer models

The orthotopic lung tumor models were allowed to develop for 2 weeks and the mice were used for *in vivo* imaging and biodistribution analysis. Free Ce6 (2.5 mg/ kg) and Ce6-CPT-UCNPs (2.5 mg/ kg of free Ce6 equivalent) were intravenously injected via the tail vein into the tumor-bearing mice. Then, the *in vivo* biodistribution and tumor targeting efficacy of each sample were evaluated by Bruker In-Vivo F PRO imaging system. Images were taken at 2h, 4h and 24h after injection and the nude mice were sacrificed by cervical vertebra dislocation 24 h after injection. Then the organs including heart, liver, spleen, lung and kidney were collected and analyzed by the imaging system. Acquisition parameters: excitation, 630/20 nm; emission, 700/30 nm.

Ce6-CPT-UCNPs for photodynamic therapy and chemotherapy of lung cancer *in vivo*

NCI-H460 subcutaneous xenografted tumor models were used in photodynamic therapy and chemotherapy. Tumor-bearing mice were used when the volume of tumors reached 50-100 mm³. The mice were divided into 5 groups (six mice each group), which were respectively treated with PBS combined with 980 nm laser irradiation (no.1 control group), free CPT (no. 2 group), free Ce6 combined with 980 nm laser irradiation (no. 3 group), Ce6-CPT-UCNPs (no.4 group), or Ce6-CPT-UCNPs combined with 980 nm laser irradiation (no.5 group). The nanoparticles or control reagents were respectively intratumorally injected at doses equivalent to 2.5 mg/kg of Ce6 and 2.5 mg/kg of CPT, and the irradiation time was set at 0. 4 h after the injection, the exposed dose was set as 980 nm laser with 0.6W/cm²for 30 min (1 min interval after each minute of irradiation). The tumor size and body weight for each mouse were recorded from no.1day to no.18 day post-injection. The therapeutic efficacy was monitored by measuring tumor volumes. Tumor volume= (tumor length) *(tumor width)²/2.

These important organs including heart, liver, spleen, lung and kidney were collected from lung tumor-bearing mice at 50 days after being treated with Ce6-CPT-UCNPs plus laser irradiation, were frozen and embeded by medium at -20° C, were sectioned in to thin slices, stained with hematoxylin and eosin(HE) stain method, and were observed by microscopy.

Biodistribution of Ce6-CPT-UCNPs in healthy nude mice

Four- to five-week-old athymic healthy nude mice were used for the biodistribution observation of Ce6-CPT-UCNPs. Ce6-CPT-UCNPs (15 mg/kg) were intravenously injected via tail vein into the mice. Then, *in vivo* and *in vitro* fluorescence imaging was performed by a Bruker In-Vivo F PRO imaging system. Images were taken at 5 h, 24 h, 72 h, 7 days and 15 days post-injection, and then the nude mice were sacrificed, the organs including heart, liver, spleen, lung and kidney were collected and analyzed by the imaging system. Acquisition parameters: excitation, 630/20 nm; emission, 700/30 nm. The organs were taken at 24 h, 7 day,15 day and 30 day, and Y element was selected as the representative element of UCNPs, and the amount of Y element in organs detected by ICP-MS(inductively coupled plasma-mass spectroscopy). Blood was taken from the heart at different times (7, 15 and 30 days) with 3 mice in each time point. Healthy mice with no injection of nanoparticles were selected as the control group. Some important hepatic function indicators such as alanine aminotransferase (ALT), aspartate aminotransferase (AST), alkaline phosphatase (ALP), two kidney function indicators such as blood urea nitrogen (BUN)) and globin (GLOB) were measured.

Statistical analysis

Mean ± SD values were used for the expression of data if there is no mention about that. Statistical analyses of data were using Student's *t* test. Differences of $P < 0.05$ were considered statistically significance.

Results and discussion

Synthesis and characterization of Ce6-CPT-UCNPs

As shown in Fig.1A, we designed light-regulated ROS-activated Ce6-CPT-UCNPs for simultaneous fluorescence imaging, chemo- and photodynamic combined therapy of lung cancer. Less than 980 nm laser irradiation, UCNPs can convert 980 nm light to 645-675 nm light, which can activate Ce6 to generate ROS for photodynamic therapy. Meanwhile, the generated ROS can quickly cleave the thioketal linker that covalently conjugated with CPT for specific

on-demand CPT drug release. To synthesize ROS-responsive CPT pro-drug, CPT was conjugated to a ROS cleavable linker (Fig.1B). The formation of CPT pro-drug was confirmed by ^{1}H NMR spectroscopy and mass spectrum (Fig.3A and Fig. S1).The mass-to-charge ratio (m/z) of 605.0 [M+Na]$^+$corresponded to ROS-responsive CPT (TL-CPT).

The UCNPs were synthesized by a thermal decomposition method from the corresponding metal trifluoroacetates in the presence of oleylamine [17]. NaYF$_4$ nanoparticles doped with Yb^{3+} as a sensitizer and Er^{3+}/Tm^{3+} as activators to display upconversion luminescence in the visible and NIR region [17]. Up to date, many ligands such as oleic acid, folic acid and carboxyl-mPEG were chosen as ligands to functionalize UCNPs [30]. In this study, carboxyl-mPEG was used to transfer hydrophobic UCNPs into aqueous phase UCNPs. Moreover, as functional ligand with –COOH, Ce6 and pro-drug TL-CPT were combined into UCNPs. The structural formula of Ce6 was shown in Fig.S2. Meanwhile, Ce6 and TL-CPT, with poor water solubility, also could be physically adsorbed on the surface of PEGylated UCNPs via hydrophobic interactions. PEGylated UCNPs has residual oleylamine layer on top of the inorganic nanoparticle beneath the PEG coating. The loading capacity of CPT and Ce6 was about 4.85%(w/w) and 5%(w/w), respectively. Our synthesis strategy allows the close binding between the UCNPs and Ce6 molecules, potentially improving effective fluorescence resonance energy transfer (FRET) between UCNPs and Ce6.

The prepared UCNPs were characterized by SEM and TEM, as shown in Fig.2A and B, prepared UCNPs were spherical shape with 25-30 nm in diameter. Dynamic light scattering (DLS) data showed aqueous size of the UCNPs was 42 nm (Fig. S3A). After Ce6-CPT-UCNPs were prepared, the size of the water-dispersible nanoparticles increased to 68 nm (Fig.S3B). Ce6-CPT-UCNPs were very stable in RPMI-1640 medium with 10% fetal calf serum within 7 days (Fig.S4). To characterize the chemical composition of the UCNPs, X-ray photoelectron spectroscopy (XPS) spectrum were performed (Fig.S5), confirming the presence of Na, Y, F and Yb in the prepared UCNPs. The elemental content of Er and Tm is too low and can't be shown in the full XPS spectrum.
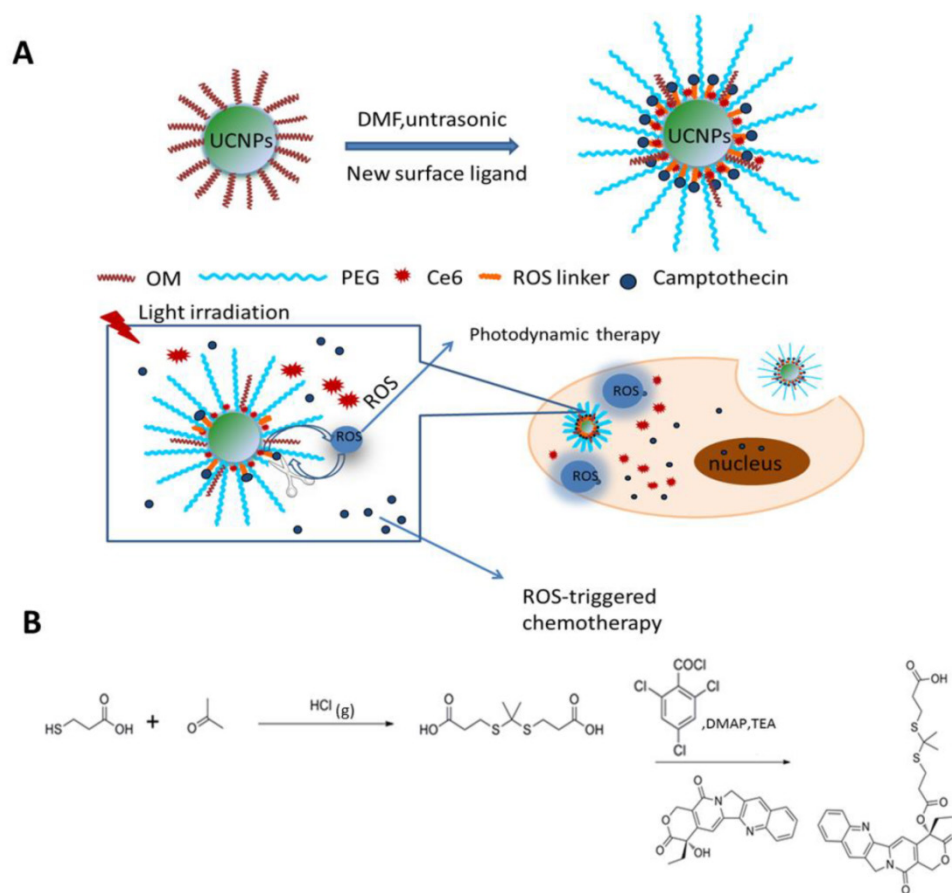

Figure 1. (A) Schematic illustration of the preparation of Ce6-CPT-UCNPs and concept of the light-regulated ROS-activated Ce6-CPT-UCNPs, OM: oleylamine. (B) Synthesis of ROS-responsive camptothecin, the product was abbreviated as TL-CPT.
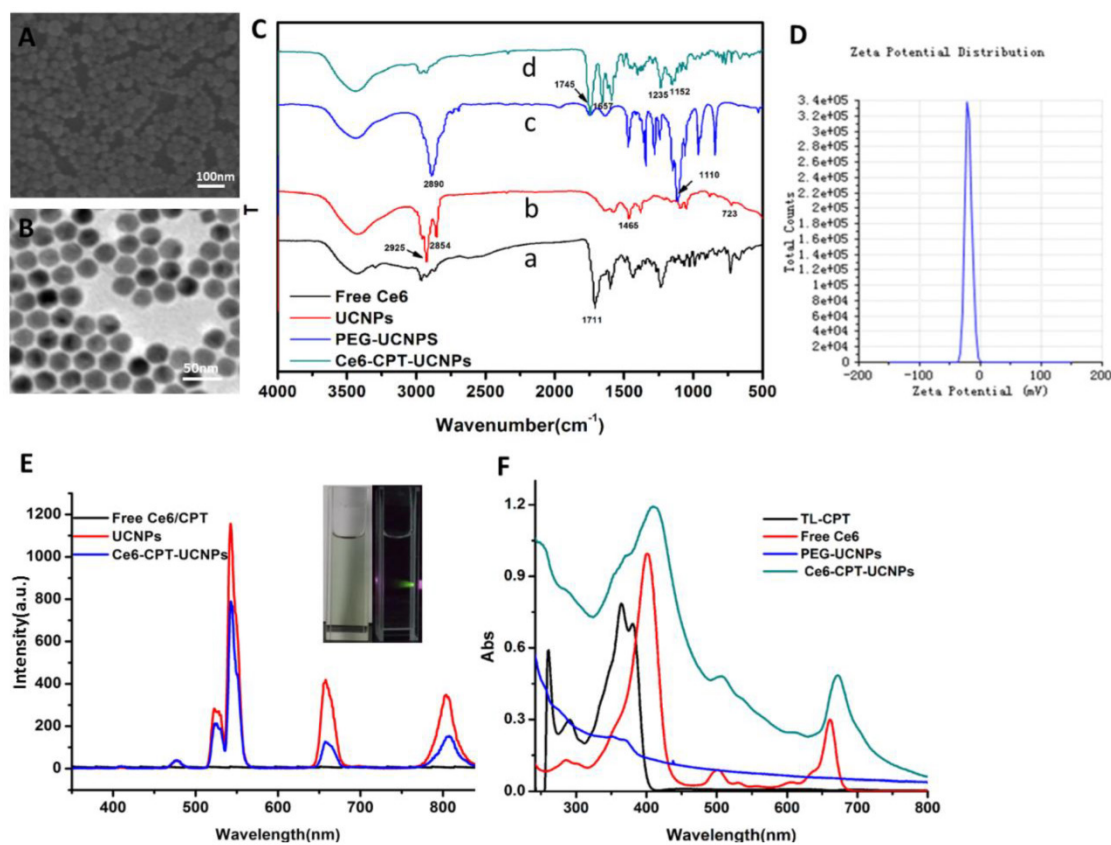
Figure 2. Characterization of Ce6-CPT-UCNPs.(A)SEM image of UCNPs.(B) TEM image of UCNPs. (C) FTIR spectra of (a) Free Ce6, (b) UCNPs, (c) PEG-UCNPs, and (d)Ce6-CPT-UCNPs.(D)Zeta potential of Ce6-CPT-UCNPs, the zeta potential was about -19.8mV. (E) Upconversion luminescence spectra of free Ce6/CPT in DMF,UCNPs (2mg/mL) and Ce6-CPT-UCNPs (2mg/mL) in water, excitation:980 nm.(F) Normalized UV/Vis absorption spectra of TL-CPT (thioketal linker conjugated with camptothecin), free Ce6, PEG-UCNPs, and Ce6-CPT-UCNPs,TL-CPT detected in DMSO solution, others dissolved in methanol.
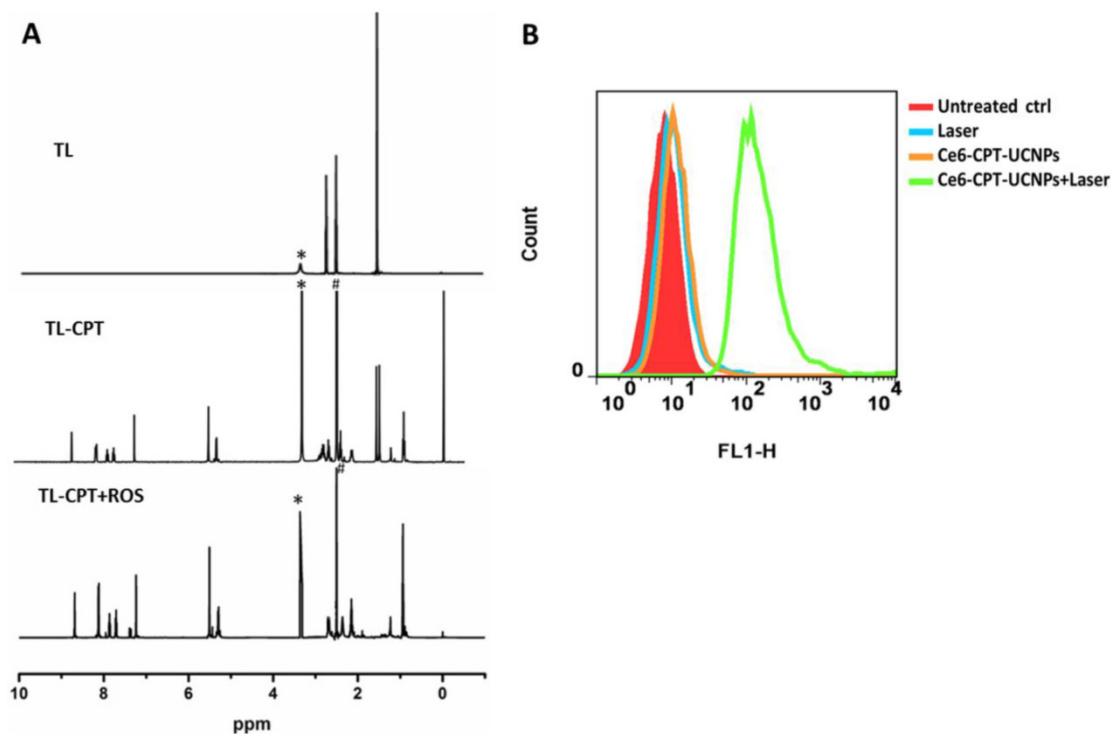

Figure 3. Characterization of ROS sensitivity and ROS generation of the Ce6-CPT-UCNPs. (A)Degradation of thioketal linkages in TL-CPT after exposure to ROS, as detected by ^{1}H NMR spectroscopy; to imitate ROS conditions, TL-CPT incubated with 400 mM H_2O_2 and 3.2μM $CuCl_2$ at 37℃ for 48 h.(B)Flow cytometric detection of ROS generation in the presence of DCFH-DA in NCI-H460 cells.

To acquire Ce6-CPT-UCNPs, important components such as Ce6, TL-CPT and mPEG-COOH were assembled onto the UCNPs. After ultrasonic treatment, the product was centrifuged, washed with water for three times and the unloaded ligands were washed off. The successful accomplishment of ligand assembly was confirmed by FTIR analysis (Fig.2C). In the FTIR spectrum of free Ce6 (Fig.2C(a)), the wide transmission band from 3300 to 2400 cm^{-1} belongs to the stretching vibration of O-H in carboxyl group and the peak at 1711 cm^{-1} corresponds to the stretching vibration of C=O in carboxyl group. Although the UCNPs were washed with cyclohexane and chloroform, it was still coated with some oleylamine. In the FTIR spectrum of UCNPs (Fig.2C(b)), the peaks at 2925cm^{-1} and 2854cm^{-1} attribute to asymmetric stretching vibration and symmetric stretching vibration of alkyl group in oleylamine, respectively. The peak at 1465 cm^{-1} is a typical bending vibration of alkyl group in oleylamine. The mPEG-COOH loaded on the UCNPs is confirmed by the peak at 1110 cm^{-1} due to the C-O-C stretch (Fig.2C(c)). In the FTIR spectrum of Ce6-CPT-UCNPs (Fig.2C(d)), the peak at 1745 cm^{-1} confirms stretching vibration of C=O in carboxyl group in Ce6. The peak at 1657 cm^{-1} belongs to the aromatic group and assures the existence of TL-CPT. The peak at 1152cm^{-1} attributes to the C-O-C stretch. Thus, Ce6, TL-CPT and PEG were successfully loaded on the UCNPs.

Zeta potential of Ce6-CPT-UCNPs was about -19.8mV (Fig.2D). The upconversion luminescence emission spectra of various samples were measured under 980 nm excitation at the same UCNPs concentration (Fig. 2E). The UCNPs have narrow emission bands located at 530-560, 645-675, and 770-830 nm. An obvious decrease in UCNPs emission intensity after Ce6 loaded was observed, particularly in its emission peak at 660 nm, which overlapped with the absorbance peak of Ce6 at the same wavelength. Such a phenomenon is likely a result of FRET between UCNPs and Ce6. In Fig.S6, the naked UCNPs didn't have any fluorescence emission from 550 nm to 850 nm (Ex:510 nm), but Ce6 had a fluorescence emission band from 650 nm to 750 nm. Therefore, Ce6 on the Ce6-CPT-UCNPs can be utilized for near infrared fluorescent imaging. Normalized UV/Vis absorption of the Ce6-CPT-UCNPs and the carboxyl ligands were shown in Fig.2F.

ROS-sensitive degradable behavior of thioketal linker

The degradation of TL-CPT under simulated ROS conditions was quantified by ^1H NMR spectra (Fig 3A). To imitate ROS condition, TL-CPT was incubated with 400 mM H_2O_2 and 3.2μM $CuCl_2$ at 37℃

.The disappearance of the thioketal linkage peak (δ=1.47, 1.54 ppm) confirmed that the thioketal linkers were efficiently cleaved by ROS, generating acetone as a by-product during the cleavage process. This result was in agreement with a previous report regarding the dethioacetalization using H_2O_2[31]. Although a short thiol linker still remain in CPT after ROS cleavage treatment, it does not affect the drug efficacy, and can be hydrolyzed in the lysosome.

We also examined the intracellular ROS production induced by Ce6-CPT-UCNPs in NCI-H460 cells via DCFH-DA staining method. DCFH-DA is a non-fluorescent cell-permeable indicator for ROS and produces fluorescence upon oxidation by ROS[32]. As expected, the Ce6 on UCNPs induced the most amounts of ROS under 980nm laser irradiation, which was detected with flow cytometry (Fig.3B). Therefore, Ce6-CPT-UCNPs could produce ROS under irradiation and could be cleaved via ROS to release chemical drug CPT.

We also investigated in vitro release course of CPT from the prepared nanoparticles in a release medium (phosphate buffered saline, PBS, pH 7.4) using dialysis bag. The in vitro release curves of CPT from Ce6-CPT-UCNPs was shown in Fig. S7.

In vitro chemo- and photodynamic therapy and cellular uptake of Ce6-CPT-UCNPs

To investigate chemo- and photodynamic combined therapeutic efficacy of Ce6-CPT-UCNPs, at first, the prepared UCNPs' cytotoxicity was evaluated by MTT assays. As shown in Fig. 4A, UCNPs showed no obvious cytotoxicity under the dose of less than 100μg/mL, even under exposed to 500μg/mL UCNPs, the cell viability was still above 80%, therefore, prepared UCNPs should be good biocompatibility.

Then, NCI-H460 cells were respectively incubated with free CPT, Ce6-UCNPs or Ce6-CPT-UCNPs, as shown in Fig. 4B, the chemo- and photodynamic treatments caused by Ce6-CPT-UCNPs resulted in lowest cell viability compared with chemo- (CPT treated group) or photodynamic treatment (Ce6-UCNP treated group) alone. After 980 nm laser irradiation being added, compared with free CPT or Ce6-UCNPs alone, cell viability in Ce6-CPT-UCNPs treated group dramatically decreased, and displayed dose-dependent decreasing effects. The phenomena could be explained as follows: the 980 nm laser excited the UCNPs to emit 645-675 nm light, and Ce6 absorbed the light to generate ROS, ROS cleaved the ROS sensitive thioketal linker to release out CPT at the same time, Ce6 and CPT killed the lung cancer cells in a synergistic way.
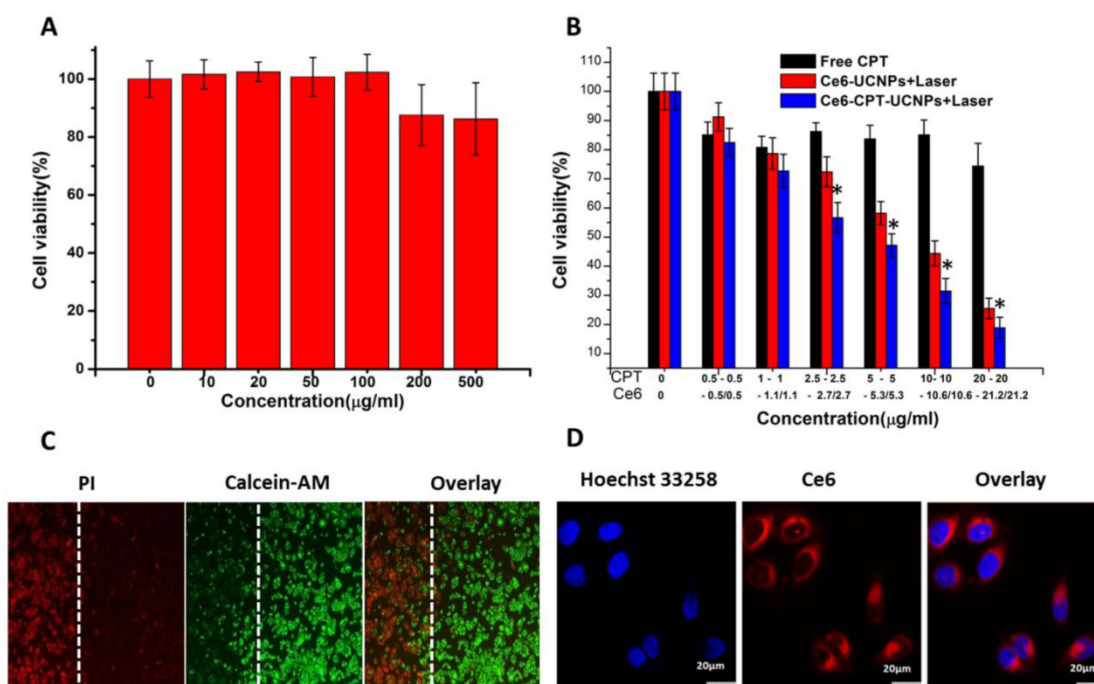
Figure 4. Cell survival analysis of NCI-H460 cells after chemotherapy, photodynamic therapy and *in vitro* cellular uptake of Ce6-CPT-UCNPs.(A) The cytotoxicity of UCNPs at different concentration. (B) Chemotherapy and photodynamic therapy of Ce6-CPT-UCNP with 980 nm laser,0.6 W/cm² for 20 min with a 1 min interval after each minute of irradiation.(C) Detection photodamage of Ce6-CPT-UCNPs by fluorescence microscopy using fluorescent probes (double-staining with PI and calcein-AM). Dead cells: red fluorescence of PI; living cells: green fluorescence of calcein-AM. The left side of the dotted line was irradiated with laser while the right side was in the dark.(D) The *in vitro* cellular uptake of Ce6-CPT-UCNPs. The data are shown as mean± SD (n =4), * indicated *P*< 0.05.

In order to observe the chemo- and photodynamic therapeutic effects directly, the treated lung cancer cells were stained with calcein-AM and PI. Living cells were visualized as green (calcein color) and dead cells were visualized as red (PI color). as shown in Fig.4C, after NCI-H460 cells incubated with Ce6-CPT-UCNPs in the dark for 4h, and then were irradiated with 980 nm laser, the dead cells with red color were only observed in the region irradiated with the laser, while those cells outside the laser irradiation region, displayed green color, were alive, which fully demonstrate that prepared Ce6-CPT-UCNPs could kill tumor cells high-efficiently under 980nm laser irradiation.

As shown in Fig.4D, confocal laser scanning microscopy images showed that Ce6-CPT-UCNPs mainly distributed in the NCI-H460 cytoplasm. This observation demonstrated that Ce6-CPT-UCNPs could be uptaken by cells and could be used for cell fluorescent imaging.

In vivo imaging and biodistribution of Ce6-CPT-UCNPs on orthotopic lung cancer models

As shown in Fig. 5A and Fig. 5B, the orthotopic lung cancer models were successfully established. The orthotopic lung tumor-bearing mouse was sacrificed and its chest was opened, confirming that the tumor grew on the lung (Fig. 5A).The CT imaging also

proved the model was successfully established (Fig. 5B). In CT photographs, the tumors on the lung existed in three different sections of the mouse lung and were marked with red and green lines. Based on the intrinsic fluorescence of Ce6, the tumor-targeting ability of Ce6-CPT-UCNPs in orthotopic lung tumor-bearing mice was evaluated using a Bruker In-Vivo F PRO imaging system. When the lung tumor-bearing mice were raised for 2 weeks, free Ce6 and Ce6-CPT-UCNPs were respectively intravenously injected via tail vein and the time dependent distribution was monitored. As shown in Fig. 5C, a large amount of Ce6-CPT-UCNPs located in the lung and liver at 2 h after injection, at 4 h and 24 h post-injection, the Ce6 fluorescence signal of Ce6-CPT-UCNPs was still strong in lung and liver, the strong Ce6 signal in lung mainly came from tumor tissues on the lung. As shown in Fig. 5D, excised tissues at 24 h post-injection were imaged, exhibited stronger fluorescence signals in the orthotopic lung tumor tissue than that of free Ce6(Fig. 5E). The strong fluorescence signal co-located in the tumor, which indicated that the Ce6-CPT-UCNPs could be used for orthotopic lung tumor imaging, which also indirectly demonstrate that Ce6-CPT-UCNPs could target in vivo lung cancer via EPR effects (enhanced permeability and retention). As a control, the free Ce6 couldn't target the lung and the free Ce6 were metabolized very quickly and cleared out.
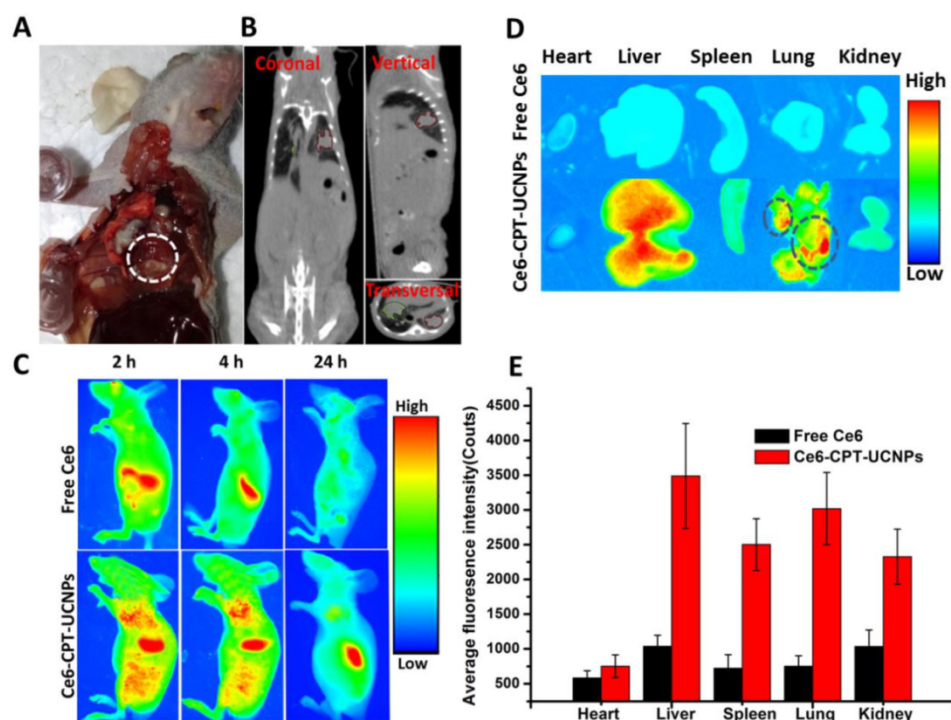
Figure 5. *In vivo* imaging and biodistribution analysis of nude mice bearing NCI-H460 orthotopic lung tumor after tail vein injection of free Ce6 or Ce6-CPT-UCNPs. (A) Established NCI-H460 orthotopic lung cancer model, the tumor was circled with dotted line. (B) CT imaging of NCI-H460 orthotopic lung nude mice,the tumors on the lung existed in three different sections of the mice and were marked with red and green line.(C) Time-lapse Ce6 fluorescence images of nude mice.(D) Fluorescence images of major organs after injection of free Ce6 orCe6-CPT-UCNPs for 24h; the tumors were circled with dotted line. (E) Semiquantitative biodistribution of free Ce6 orCe6-CPT-UCNPs in nude mice determined by the average Ce6 fluorescence intensity of organspost-injection for 24 h. The data are shown as mean± SD.

In vivo chemo- and photodynamic therapy and potential toxic side-effect evaluation

To evaluate the chemo- and photodynamic therapeutic efficiency of Ce6-CPT-UCNPs *in vivo*, a single dose of PBS, free CPT, free Ce6, and Ce6-CPT-UCNPs were respectively injected into tumor-bearing mice when the tumor size grew to 50–100 mm^3. After 4 h post-injection, these mice treated respectively with PBS, free Ce6 and Ce6-CPT-UCNPs were irradiated at the tumor site with 980 nm laser for 30 min ($0.6W/cm^2$,1 min interval after each minute of irradiation). As shown in Fig.6A and B, the tumors treated with PBS plus laser irradiation grew rapidly, suggesting the growth of NCI-H460 tumors was not affected by laser irradiation. The growth of NCI-H460 tumors treated with free Ce6 and free CPT was slightly inhibited after laser irradiation. Although CPT is a well-known chemotherapeutic agent for tumor treatment, it usually requires multiple and high doses to achieve a satisfactory therapeutic effect. Notably, free Ce6 plus laser irradiation to treat tumor couldn't effectively inhibit tumor growth, which is because the 980 nm laser cannot activate Ce6 to produce ROS, therefore, cannot kill the tumor cells. However, the Ce6 dye was intratumorally injected, the concentration of Ce6 was high and the color of the Ce6 was deep. The Ce6 with deep color could absorb very less 980 nm laser to elevate local temperature to

inhibit the tumor growth.

The tumor treated with Ce6-CPT-UCNPs and no laser irradiation did not become smaller, which is because Ce6-CPT-UCNPs without laser irradiation were not activated, Ce6 and CPT in the Ce6-CPT-UCNPs cannot be released out, and cannot kill tumor cells. The tumor treated with Ce6-CPT-UCNPs plus laser irradiation became gradually small, and finally completely disappeared, only a small un-healing wound existed on the tumor site, which healed completely at two weeks after treatment with laser irradiation. No tumor recurrence and metastasis was observed in this group within 50 days after treatment. This is because that 980 nm laser irradiation excited UCNPs to emit 645-675 nm laser and Ce6 absorbed the laser to release enough ROS, the ROS could cleave the thioketal linker to release camptothecin, which killed the tumor cells via chemotherapy and phototoxicity means at the same time. Compared with 630 nm laser, 980 nm laser has higher light penetration depth in biological tissues, enhancing the therapeutic efficacy of Ce6-CPT-UCNPs. Compared with other groups such as PBS plus laser irradiation, free Ce6, free CPT, and Ce6-CPT-UCNPs plus no laser irradiation, tumor sizes existed statistical difference between the Ce6-CPT-UCNPs plus 980nm laser irradiation group and other group ($P<0.05$),which fully show that Ce6-CPT-UCNPs plus

980nm laser irradiation can treat lung cancer high efficiently.

We further investigated the toxic side effect of Ce6-CPT-UCNPs on NCI-H460 tumor bearing mice. The loss of body weight was selected as an indicator of treatment-induced toxicity. As shown in Fig. 7A, Ce6-CPT-UCNPs plus laser treatment group caused mouse body weight variation, bout the body weight returned to normal status at 3 weeks after treatment. These important organs collected from lung tumor-bearing mice at 50 days after being treated with Ce6-CPT-UCNPs plus laser irradiation, were sectioned in to thin slices, stained with hematoxylin and eosin(HE) stain method, and were observed by microscopy. As shown in Fig.7B, no obvious abnormality were observed in liver, spleen, lung, kidney tissue slices. These data highly suggest that the prepared Ce6-CPT-UCNPs under a single-dose treatment did not cause significant side effects to important organs.

In vivo biodistribution and hepatic and renal toxicity evaluation on healthy mice

In order to observe *in vivo* biodistribution of prepared Ce6-CPT-UCNPs, healthy athymic nude mice were injected with 15 mg/kg of Ce6-CPT-UCNPs via the tail vein [33]. At different time points post-injection, mice were anesthetized, sacrificed, and imaged by animal imaging system (Fig.S8). At 5 h post-injection, the fluorescence signals mainly distributed in liver, lung and kidney. Within 24 h post-injection, fluorescent signal intensity in spleen organ was gradually increased, while fluorescence signal intensities in liver, lung and kidney gradually decreased. At 24 h post-injection, this fluorescent signal intensity difference was biggest between the spleen and the liver, which may be due to the spleen being the largest immune organ. At 7 days post-injection, the fluorescence signal was significantly reduced in the mice. At 15 days post-injection, almost no fluorescence signal was detected in the mice compared with the control mice. The results were also further confirmed by the measurement of the Y element concentration in organs by ICP-MS (Fig.8A). ICP-MS analysis showed Ce6-CPT-UCNPs' uptake and retention took place primarily in the liver and spleen, partial Ce6-CPT-UCNPs accumulated in lung within 24 h post-injection.
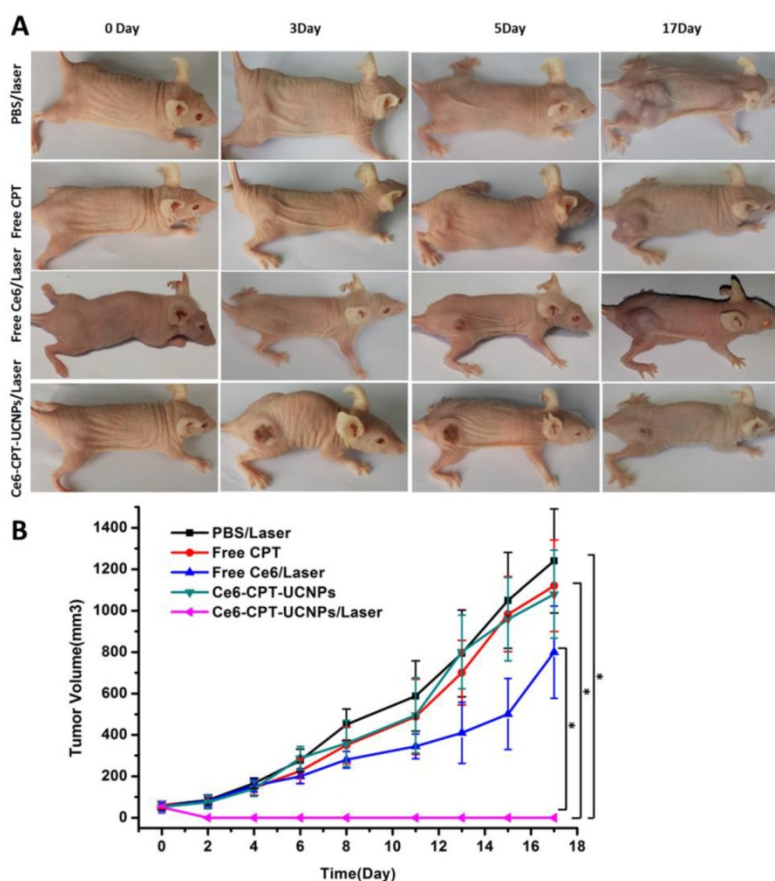

Figure 6. *In vivo* chemo- and photodynamic therapyof the Ce6-CPT-UCNPs. (A) Images of mice bearing NCI-H460 tumors before and after treatments. The mice were irradiated by 980 nm laser with a power density of 0.6W/cm^2 for 30 min (1 min interval after each minute of irradiation). (B) NCI-H460 tumor growth curves of different groups after treatments. The data are shown as mean ±SD (n = 6), * indicated *P*< 0.05.
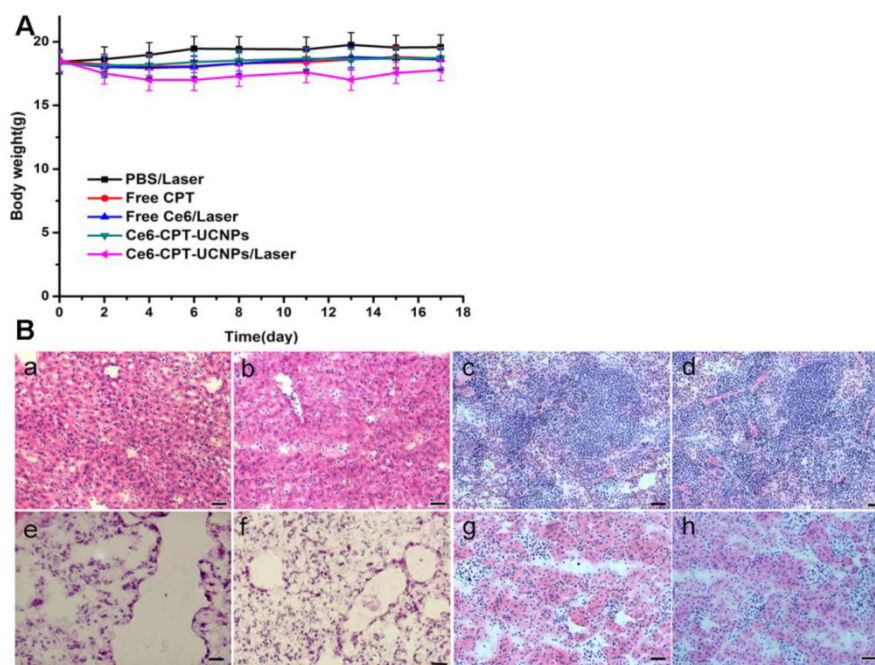
Figure 7. No obvious toxic effect was observed for Ce6-CPT-UCNPs plus laser treated mice. (A) Body weight curves after various treatments. (B) H&E stained images of major organs; (a)(c)(e)(g)Liver, spleen, lung and kidney of healthy mice;(b)(d)(f)(h)Liver, spleen, lung and kidney of Ce6-CPT-UCNPs plus laser treated mice; Scale bar = 25 μm, 50 days after Ce6-CPT-UCNPs plus laser treatment, the mice were sacrificed and no noticeable abnormality was observed in liver, spleen, kidney and lung.
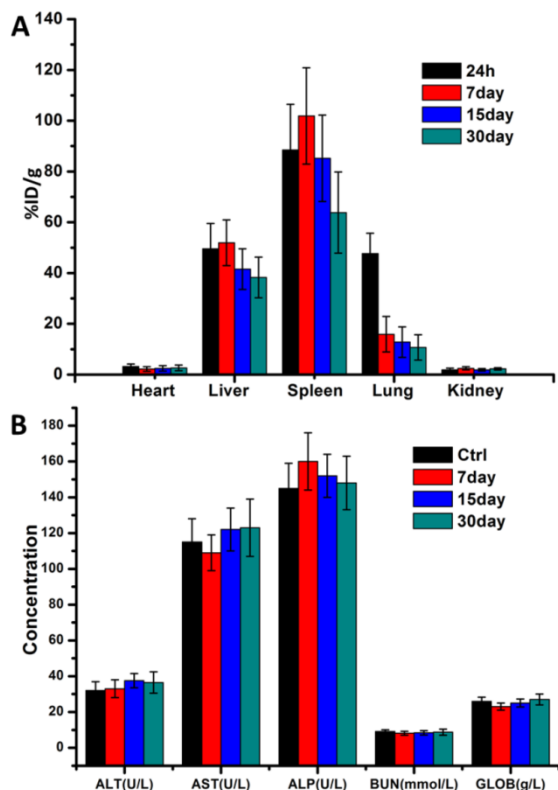

Figure 8. *In vivo* biodistribution analysis and hepatic and renal toxicity evaluationon healthy mice.(A)Biodistribution of nanoparticles in organs of mice with intravenous injection of Ce6-CPT-UCNPs (15 mg/kg) at different time points.(B) Blood biochemistry analysis of mice treated with Ce6-CPT-UCNPs at day 7, 15, and 30 after i.v. injection. The data are shown as mean ±SD (n = 3).

In order to confirm whether prepared Ce6-CPT-UCNPs cause damages to liver and kidney, five important biochemical markers were measured by ELISA kit. As shown in Fig.8B, the three important hepatic function indicators such as alanine aminotransferase (ALT), Aspartate aminotransferase (AST) and alkaline phosphatase (ALP), had no significant difference between the control mice and the mice exposed to Ce6-CPT-UCNPs at 30 days after treatment. The kidney function indicators such as blood urea nitrogen (BUN) and globin (GLOB) had no significant difference between the control mice and the mice treated with Ce6-CPT-UCNPs at 30 days after treatment. These results show that prepared Ce6-CPT-UCNPs under the dose of 15 mg/kg may be safety for mice without 980 nm laser irradiation.

Conclusions

In summary, a thioketal linker based ROS responsive pro-drug Ce6-CPT-UCNPs was successfully prepared, and was confirmed to be able to produce ROS under 980nm laser irradiation, ROS could cleave the thioketal linker and released out chemical drug CPT, exhibited combined chemo- and photodynamic therapy function, and simultaneous fluorescent imaging function. The prepared Ce6-CPT-UCNPs under 980 nm laser irradiation were successfully used for fluorescence imaging, and simultaneous combined chemo-and photodynamic therapy of lung cancer. This should be first report. Our results also show that

prepared Ce6-CPT-UCNPs mainly distributed in liver and spleen organs of healthy mice, and gradually disappeared at 15 days post-injection, did not show obvious toxic side-effects to important organs such as heart, liver, spleen, lung and kidney under no 980 nm laser irradiation. For in situ lung cancer-bearing mice models, prepared Ce6-CPT-UCNPs could gather in the orthotopic lung cancer site highly efficiently by EPR effect. For subcutaneous lung cancer-bearing mice model, after being injected intratumorally with prepared Ce6-CPT-UCNPs, under 980 nm laser irradiation, tumor growth was inhibited markedly, even tumor disappeared via combined chemo-and photodynamic therapy effects, no tumor recurrence and metastasis were observed at 50 days after treatment. This should be first report. In all, high performance Ce6-CPT-UCNPs own great potential in applications such as simultaneous lung cancer fluorescent imaging, ROS-activated chemo-, and photodynamic therapy in the near future.

Abbreviations

ROS: reactive oxygen species; TL-CPT: thioketal linker to camptothecin; UCNPs: upconversion nanoparticles; NIR: near-infrared; ALT: alanine aminotransferase; AST: Aspartate aminotransferase; ALP: alkaline phosphatase; BUN: blood urea nitrogen; GLOB: globin.

Supplementary Material

Figures S1-S8. http://www.thno.org/v06p0456s1.pdf

Acknowledgements

Competing Interests

Authors claim no financial competent interest.

References

1. Muthu MS, Leong DT, Mei L, Feng SS. Nanotheranostics -application and further development of nanomedicine strategies for advanced theranostics. Theranostics.2014; 4: 660-77.
2. Phillips WT, Bao AD, Brenner AJ, Goins BA. Image-guided interventional therapy for cancer with radiotherapeutic nanoparticles. Adv Drug Deliver Rev. 2014; 76: 39-59.
3. Park YI, Kim HM, Kim JH, Moon KC, Yoo B, Lee KT, et al. Theranostic probe based on lanthanide-doped nanoparticles for simultaneous in vivo dual-modal imaging and photodynamic therapy. Adv Mater. 2012; 24: 5755-61.
4. Yue C, Liu P, Zheng M, Zhao P, Wang Y, Ma Y, et al. IR-780 dye loaded tumor targeting theranostic nanoparticles for NIR imaging and photothermal therapy. Biomaterials.2013; 34: 6853-61.
5. Dong Y, Yang J, Liu H, Wang T, Tang S, Zhang J, et al. Site-specific drug-releasing polypeptide nanocarriers based on dual-pH response for en-hanced therapeutic efficacy against drug-resistant tumors. Theranostics.2015; 5: 890-904.
6. Liu P, Yue CX, Sheng ZH, Gao GH, Li MX, Yi HQ, et al. Photosensitizer-conjugated redox-responsive dextran theranostic nanoparticles for near-infrared cancer imaging and photodynamic therapy. Polym Chem. 2014; 5: 874-81.
7. Roy D, Brooks WLA, Sumerlin BS. New directions in thermoresponsivepolymers. ChemSoc Rev. 2013; 42: 7214-43.
8. Li N, Li N, Yi QY, Luo K, Guo CH, Pan DY, et al. Amphiphilic peptide dendritic copolymer-doxorubicin nanoscale conjugate self-assembled to enzyme-responsive anti-cancer agent. Biomaterials.2014; 35: 9529-45.
9. Chen LF, Wang WQ, Su B, Wen YQ, Li CB, Zhou YB, et al. A light-responsive release platform by controlling the wetting behavior of hydrophobic surface. Acs Nano. 2014; 8: 744-51.
10. Fomina N, Sankaranarayanan J, Almutairi A. Photochemical mechanisms of light-triggered release from nanocarriers. Adv Drug Deliver Rev. 2012; 64: 1005-20.
11. Shim MS, Xia YN. A Reactive Oxygen Species (ROS)-responsive polymer for safe, efficient, and targeted gene delivery in cancer cells. AngewChemInt Edit.2013; 52: 6926-9.
12. Yuan YY, Liu J, Liu B. Conjugated-polyelectrolyte-based polyprodrug: targeted and image-guided photodynamic and chemotherapy with on-demand drug release upon irradiation with a single light source. AngewChemInt Edit.2014; 53: 7163-8.
13. Trachootham D, Alexandre J, Huang P. Targeting cancer cells by ROS-mediated mechanisms: a radical therapeutic approach? Nat Rev Drug Discov.2009; 8: 579-91.
14. Wagner A, Denzer UW, Neureiter D, Kiesslich T, Puespoeck A, Rauws EA, et al. Temoporfin improves efficacy of photodynamic therapy in advanced biliary tract carcinoma: A multicenter prospective phase II study. Hepatology. 2015.
15. Choudhary S, Nouri K, Elsaie ML. Photodynamic therapy in dermatology: a review. Laser Med Sci. 2009; 24: 971-80.
16. Zhang CL, Li C, Liu YL, Zhang JP, Bao CC, Liang SJ, et al. Gold nanoclusters-based nanoprobes for simultaneous fluorescence imaging and targeted photodynamic therapy with superior penetration and retention behavior in tumors. AdvFunct Mater.2015; 25: 1314-25.
17. Liu Q, Sun Y, Li C, Zhou J, Yang T, Zhang X, et al. 18F-labeled magnetic-upconversion nanophosphors via rare-earth cation-assisted ligand assembly. Acs Nano. 2011; 5: 3146-57.
18. Wang K, Ma J, He M, Gao G, Xu H, Sang J, et al. Toxicity assessments of near-infrared upconversion luminescent LaF3:Yb,Er in early development of zebrafish embryos. Theranostics.2013; 3: 258-66.
19. Qiu P, Zhou N, Chen H, Zhang C, Gao G, Cui D. Recent advances in lanthanide-doped upconversion nanomaterials: synthesis, nanostructures and surface modification. Nanoscale.2013; 5: 11512-25.
20. Gao G, Zhang CL, Zhou ZJ, Zhang X, Ma JB, Li C, et al. One-pot hydrothermal synthesis of lanthanide ions doped one-dimensional upconversion submicrocrystals and their potential application in vivo CT imaging. Nanoscale.2013; 5: 351-62.
21. Wang C, Tao HQ, Cheng L, Liu Z. Near-infrared light induced in vivo photodynamic therapy of cancer based on upconversion nanoparticles. Biomaterials.2011; 32: 6145-54.
22. Jalil RA, Zhang Y. Biocompatibility of silica coated NaYF4 upconversion fluorescent nanocrystals. Biomaterials.2008; 29: 4122-8.
23. Xiong LQ, Yang TS, Yang Y, Xu CJ, Li FY. Long-term in vivo biodistribution imaging and toxicity of polyacrylic acid-coated upconversionnanophosphors. Biomaterials.2010; 31: 7078-85.
24. Park Y, Kim HM, Kim JH, Moon KC, Yoo B, Lee KT, et al. Theranosticprobe-based on Lanthanide-doped nanoparticles for simultaneous in vivo dual-modal imaging and photodynamic therapy. Adv Mater. 2012; 24: 5755-61.
25. Zhou L, Wang R, Yao C, Li XM, Wang CL, Zhang XY, et al. Single-band upconversio nnanoprobes for multiplexed simultaneous in situ molecular mapping of cancer biomarkers. Nat Commun. 2015; 6.
26. Wang X, Liu K, Yang GB, Cheng L, He L, Liu YM, et al. Near-infrared light triggered photodynamic therapy in combination with gene therapy using upconversion nanoparticles for effective cancer cell killing. Nanoscale.2014; 6: 9198-205.
27. Yang S, Li NJ, Liu Z, Sha WW, Chen DY, Xu QF, et al. Amphiphilic copolymer coated upconversion nanoparticles for near-infrared light-triggered dual anticancer treatment. Nanoscale.2014; 6: 14903-10.
28. O'Connor AE, Gallagher WM, Byrne AT. Porphyrin and nonporphyrin photosensitizers in oncology: preclinical and clinical advances in photodynamic therapy. PhotochemPhotobiol. 2009; 85: 1053-74.
29. Roberts JE. Lanthanum and neodymium salts of trifluoroaceticacid. J Am Chem Soc. 1961; 83: 1087-8.
30. Chien YH, Chou YL, Wang SW, Hung ST, Liau MC, Chao YJ, et al. Near-infrared light photocontrolled targeting, bioimaging, and chemotherapy with caged upconversion nanoparticles *in vitro* and *in vivo*. Acs Nano. 2013; 7: 8516-28.
31. Ganguly NC, Mondal P. Mild, efficient, and greener dethioacetalizationprotocolusing 30% hydrogen peroxide in catalytic combination with ammonium iodide. Synthetic Commun.2011; 41: 2374-84.

32. Zhang CL, Zhou ZJ, Zhi X, Ma Y, Wang K, Wang YX, et al. Insights into the distinguishing stress-induced cytotoxicity of chiral gold nanoclusters and the relationship with GSTP1. Theranostics.2015; 5: 134-49.

33. Yang K, Wan JM, Zhang S, Zhang YJ, Lee ST, Liu Z. In vivo pharmacokinetics, long-term biodistribution, and toxicology of PEGylated graphene in mice. Acs Nano. 2011; 5:516-22.